Effects of platinum high-temperature redispersion on Pt/Al$_2$O$_3$ diesel oxidation catalyst for nitric oxide oxidation and its reaction pathway

Bin Gao [a], Na Zhang [a], Huangwei Zhang [b,c], Run Qiu [a], Zhi Chen [a], Yunxiang Li [a], Zhengzheng Yang [a,*]

[a] College of Environmental Science and Engineering, China West Normal University, Nanchong 637009, China
[b] Department of Mechanical Engineering, National University of Singapore, 9 Engineering Drive 1, Singapore 117576, Singapore
[c] Advanced Manufacturing and Materials Centre, National University of Singapore, Chongqing Research Institute, Chongqing 401123, China

A B S T R A C T

High-temperature redispersion of platinum nanoparticle is inevitable for Pt/Al$_2$O$_3$ diesel oxidation catalyst (DOC), yet its effects on NO catalytic oxidation and its reaction mechanism are still indeterminate. Results of this work indicate that high-temperature redispersion not only decrease the nano-size of platinum particle, but also increase the crystallinity. The smaller size of platinum nanoparticle is beneficial for the reduction of high valence Pt$^{\delta+}$ species to form Pt^0 active phase and hence improving NO oxidation performance. The higher crystallinity of platinum particle is beneficial to maintaining Pt^0 state but adverse to the reduction of Pt$^{\delta+}$ species during long-time use. *In-situ* Fourier transform infrared spectroscopy results prove that NO oxidation on Pt/Al$_2$O$_3$ catalyst is mainly through the intermediates of nitrite and bridging nitrate. It will convert to chelated nitrates if the decomposition of nitrite and bridging nitrate intermediates are not able to occur promptly. Chelated nitrates are stable and hard to decompose which therefore will restrain NO oxidation reaction. The smaller Pt nano-size is conducive to the decomposition of nitrite/nitrate intermediates and therefore boost NO oxidation reaction, simultaneously the higher Pt crystallinity will lead to the generation and accumulation of chelated nitrates consequently cover the active sites and restrain NO oxidation reaction.

1. Introduction

Diesel engines have played an important role in transportation industry due to the higher durability, fuel efficiency, power performance and less carbon dioxide emissions [1,2]. However, air pollutants, *e.g.* carbon monoxide (CO), unburned hydrocarbon (UHC), nitric oxides (NO$_x$) and particulate matters (PM), from the diesel engines would cause serious atmospheric pollution and human health risk [3,4]. To reduce the pollutants from diesel exhaust and meet the increasingly stringent exhaust emission standards, modern vehicles have to be equipped with an exhaust gas aftertreatment system comprising of monolithic catalytic convertors [5,6]. The system usually includes at least three devices: diesel oxidation catalyst (DOC) for CO, UHC and NO oxidation; diesel particulate filter (DPF) for removal of PM and selective reduction catalyst (SCR) for de-NO$_x$ [7–9]. In particular, catalytic NO oxidation to NO$_2$ on DOC can simultaneously promote the low-temperature elimination of soot and NO$_x$ on the downstream DPF and SCR [10,11].

Since the noble metal of platinum has good chemical poison resistance and high catalytic oxidation activity [12]. Considering the sulfur poison and SO$_4^{2-}$ effect on catalyst in the exhaust [13–15] and the need of high NO catalytic oxidation performance, platinum-based catalyst has been extensively studied and used as DOC catalysts [16–18]. It is well known that the relatively smaller platinum nanoparticles usually have more surface Pt atoms, thereby high active sites of edges and corners and higher catalytic performances [19–22]. However, for the NO oxidation reaction on Pt-supported DOC catalysts, the catalyst with relatively larger Pt nanoparticle generally shows a higher catalytic activity. This is mainly because metallic Pt^0 is the active species for NO oxidation reaction, and the larger Pt nanoparticle maintains Pt^0 metal state more easily under oxidative conditions, and therefore has more Pt^0 active sites [23–27]. Our previous works [28–30] have shown that the high valence Pt$^{\delta+}$ (PtO and PtO$_2$) on DOC catalyst can be reduced to form Pt^0 active species by the trace amount of CO, UHC and even NO during the long-term application. Moreover, the smaller Pt nanoparticle can be reduced to form Pt^0 active species more easily and hence promote the NO oxidation activity. It is worthy to note that the

catalyst Pt particle size is not unchangeable during the long-term reaction process. High-temperature sintering and redispersion of Pt nanoparticle always proceed during the whole reaction process [31–33]. However, till now the effects of high-temperature redispersion of Pt-based DOC catalyst on NO oxidation performance and especially its reaction pathway is still inconclusive. In this work, typical Pt/Al$_2$O$_3$ was used as model DOC catalyst, and the effects of Pt nanoparticle high-temperature redispersion on catalyst physicochemical properties and the consequently catalytic NO oxidation performance as well as reaction pathway were investigated systematically.

2. Experimental method

2.1. Catalyst preparation

The Pt/Al$_2$O$_3$ catalyst is prepared by impregnating Pt(NO$_3$)$_2$ solution on the commercial Al$_2$O$_3$ support (Solvay S.A., ~120 m^2/g, contains a small proportion of SiO$_2$) and then calcining at different temperature. Firstly, the Al$_2$O$_3$ was calcined in a muffle furnace at 800 °C for 3 h so as to eliminate the effects of support texture properties. Then, the calculated amount of Pt(NO$_3$)$_2$ solution (Heraeus Group, Pt, 28.25 wt%) was dissolved in deionized water to obtained Pt(NO$_3$)$_2$ precursor solution (~0.04 mol/L), and then impregnated on the Al$_2$O$_3$ with a Pt loading amount of 1.0 wt%. After drying for 12 h at 80 °C, the sample was evenly divided into four parts and separately calcinated in muffle furnace at 500 °C, 600 °C, 700 °C, and 800 °C, respectively in atmosphere for 3 h. Finally, the obtained Pt/Al$_2$O$_3$ powder catalyst was labeled as D500, D600, D700, and D800, respectively.

2.2. Catalytic performance test

The catalytic performance of all the catalysts was measured in a multi-gas path fixed-bed catalyst evaluation device. Firstly, approximately 0.45 g of the granular catalyst was filled into the catalytic reaction tube. Then, the simulated diesel vehicle exhaust gases (CO 1000 ppm, C$_3$H$_6$ 330 ppm, NO 1000 ppm, CO$_2$ 8.0 vol%, steam 7.0 vol%, O$_2$ 10.0 vol% and N$_2$ balance) were introduced in the reactor with a gas hourly space velocity (GHSV) of 80000 mL·g^{-1}·h^{-1}. After that the reactor was heated to 500 °C by 10 °C·min^{-1}; meanwhile, the outlet NO and NO$_2$ concentrations were detected by a flue gas analyzer (MRU NOVA PLUS, Germany), and the test results were marked with a postfix of -fresh (such as D500-fresh). And then to study the NO catalytic oxidation performance of the catalyst during long-term use, the fresh catalyst was pre-treated at 500 °C for 3 h in the simulated diesel vehicle exhaust conditions. Afterwards, it is naturally cooled down to room temperature, and then the reactor was heated to 500 °C by 10 °C·min^{-1} again, and the NO and NO$_2$ concentrations were detected. The test was repeated several times (2–4 times) until the NO oxidation ratio curves were constant, and the test results were labeled with a postfix of -cycle1/-cycle2/-cycle3/-cycle4 (such as D500-cycle1).

2.3. Catalyst characterization

The nanosized morphology and structure of the catalyst were characterized by a high-resolution transmission electron microscope (HR-TEM) of Thermo Fisher Scientific FEI TALOS F200.

X-ray diffraction (XRD) experiment was performed on a Rigaku Ultima IV diffractometer using Cu Kα radiation (λ = 0.15405 nm) with a scanning step of 0.05°/min. The crystalline phases were identified by comparison with the reference from the International Center for Diffraction Data (ICDD).

X-ray photoelectron spectroscopy (XPS) data were collected on Thermo Scientific ESCALAB 250xi with an Al Kα source (hv = 1486.6 eV) operated at 12.5 kV and 16 mA. The passing energy is 20 eV, number of scans is more than 5, scanning resolution is 0.05 eV. The binding energies of XPS spectra were calibrated using C1s at 284.80 eV.

Nitrogen adsorption-desorption tests were performed on a Micrometrics ASAP 2460 automatic micropore physisorption analyzer. Before the test, all samples were pretreated at 300 °C for 3 h under vacuum.

Hydrogen temperature-programmed reduction (H$_2$-TPR) test was carried out on a fixed-bed TPR dynamic adsorption apparatus. Firstly, about 100 mg sample was placed in a quartz reaction tube and pretreated at 450 °C in N$_2$ gas stream for 30 min. After it was cooled down to room temperature, we switched on the N$_2$ flow to achieve a gas mixture of 5% H$_2$-95% N$_2$ (40 mL·min^{-1}), and then heat the reactor to 900 °C at a rate of 10 °C·min^{-1}. The H$_2$ consumption signal was detected by a TCD and the amounts were calibrated by the reduction of pure CuO.

NO temperature-programmed desorption (NO-TPD) was performed on a dynamic adsorption apparatus. About 100 mg sample was placed in a quartz tube reactor and purged under 40 mL/min of He flow at 450 °C for 30 min and then being cooled down to room temperature. Afterwards, the sample was exposed to a 40 mL/min gas flow of 2.5 vol% NO-He at 80 °C for 1 h. Subsequently, the sample was purged with 40 mL/min He flow for 30 min to remove the excess adsorbed oxygen. Finally, the sample was heated from 80° to 900 °C with a rate of 10 °C/min under 40 mL/min He flow. The NO desorption pattern was recorded by a TCD.

The *in-situ* Fourier transform infrared spectroscopy (*in-situ* FT-IR) spectra were collected on a Fourier transform infrared spectrometer (Thermo Scientific Nicolet iS 50, America) with MCT detector. Firstly, all the catalysts were pretreated at 120 °C overnight to remove the impurities adsorbed on catalysts. Then, about 50 mg sample of 1:50 catalyst and KBr was pressed to a tablet under infrared baking lamp, and then heated at 120 °C for 30 min. After that the sample was placed in the reaction cell. The tests were performed under both the NO-only and simulated diesel exhaust environments. For the NO-only environments, NO (1000 ppm)-N$_2$ mixture (0.1 MPa) was introduced in the sample for 2 min, after that the reaction cell was evacuated to 5.0 × 10^{-5} h Pa. Then the O$_2$ (10.0 vol%)-N$_2$ mixture (0.1 MPa) was introduced in the catalyst and the *in-situ* FT-IR spectra were collected. For the simulated diesel exhaust environments, CO (1000 ppm)-C$_3$H$_6$ (330 ppm)-NO (1000 ppm)-CO$_2$ (3000 ppm)-N$_2$ mixture (0.1 MPa) was introduced in the sample for 2 min, after that the reaction cell was evacuated to 5.0 × 10^{-5} h Pa. Then the O$_2$ (10.0 vol%)-N$_2$ mixture (0.1 MPa) was introduced in the catalyst and the *in-situ* FT-IR spectra were collected.

3. Results and discussion

3.1. Catalytic performance

NO oxidation ratio curves of all the catalysts under simulated diesel exhaust gases conditions are shown in Fig. 1. Because the catalytic oxidation of CO and C$_3$H$_6$ on the Pt-based diesel oxidation catalyst are far lower than 200 °C as reported by our previous work.[29,34–36] The catalytic elimination of CO and C$_3$H$_6$ can be occurred easily in the diesel exhaust temperature range (200–400 °C), so this work mainly focuses on the catalytic oxidation of NO. Firstly, the catalytic NO oxidation test on the freshly prepared catalyst was performed and marked with the postfix of -fresh. Then the catalyst was continuously used for 3 h at 500 °C under the simulative diesel vehicle exhaust conditions and subsequently retested the NO oxidation performance several times until the catalytic activity is consistent, and the sample was marked with the postfix of -cycle1/2/3/4, respectively. The oxidation product of NO is mainly NO$_2$, and other nitrogen oxides are not detected. As shown in Fig. 1, the NO oxidation ratio of all the catalysts firstly increased with the rise of reaction temperature. When the reaction temperature continues rising, the NO oxidation ratio reaches the peak and then gradually decreases because of the thermodynamic limitations [16,37]. For all the catalysts, the starting temperatures of NO oxidation are similar (at around 235 °C) under the simulative diesel vehicle exhaust conditions. The light-off temperature ($T_{10\%}$, the temperature when NO oxidation ratio reaches to 10%) of all samples are also generally similar, the $T_{10\%}$ of all the fresh catalysts are approximately 275 °C. However, the peak temperature (T_P,
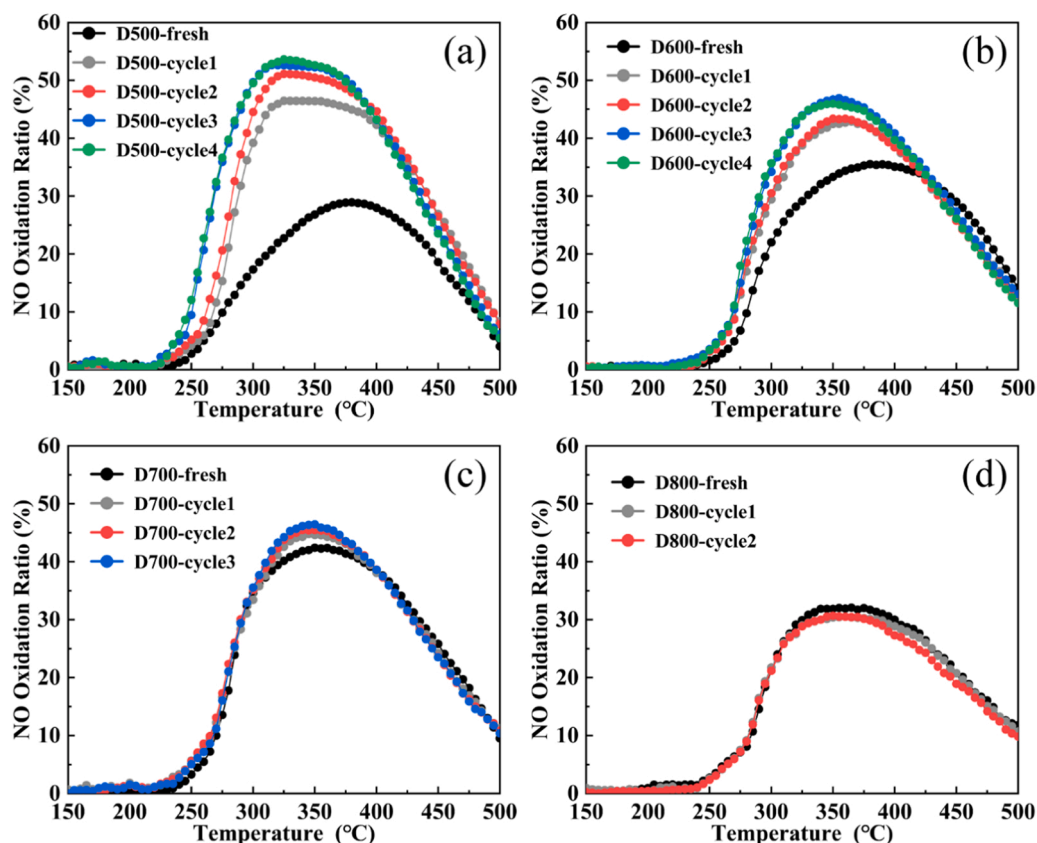
Fig. 1. NO oxidation ratio on the catalysts: (a) D500, (b) D600, (c) D700 and (d) D800.

the temperature when NO oxidation ratio reaches to peak) and the maximum conversion ratio of NO to NO_2 (max of NO oxidation ratio) of the catalysts show a significant difference. It indicates that the catalyst can promote NO oxidation when the starting temperature was reached and can affect the max value of NO oxidation ratio. The $T_{10\%}$, T_P and max of NO oxidation ratio are summarized in Table 1.

The T_P of D500-fresh, D600-fresh, D700-fresh and D800-fresh are approximately 375 °C, 380 °C, 360 °C and 365 °C, respectively. The max of NO oxidation ratio for the D500-fresh, D600-fresh, D700-fresh and D800-fresh are about 28.9%, 35.5%, 42.4% and 32.0%, respectively. It can be seen that the peak temperature (T_P) of NO oxidation on the fresh catalysts generally decrease with the catalyst treatment temperature, and the max of NO oxidation ratio for all the fresh catalyst obviously increase with the treatment temperature, except the D800-fresh. It indicates that the initial NO catalytic oxidation performance of Pt/Al_2O_3 can be obviously enhanced by the high-temperature treatment, and excessively high treatment temperature (~800 °C) will inhibit NO catalytic oxidation activity.

After the initial NO catalytic oxidation test, the catalyst was

continuously used for 3 h at 500 °C in the simulative diesel vehicle exhaust gases, and subsequently retested the NO oxidation performance until the NO oxidation ratio curves are consistent. Generally, during the long-time and multiple catalytic reaction under simulated diesel exhaust conditions, the catalytic NO oxidation activity of all the prepared catalysts are continually getting better and then becoming stable. This is mainly because of the reduction of high-valence $Pt^{\delta+}$ species to Pt^0 active sites in the long-time reactions, as reported in our previous work [28,29]. As shown in Fig. 1(a), the NO catalytic oxidation activity of the D500 catalyst shows an obvious enhancement during the long-time use (multiple NO oxidation test cycles), not only the max NO oxidation ratio increased, but also the NO oxidation reaction of $T_{10\%}$ and T_P decreased. Fig. 1(b) and Fig. 1(c) display that the NO catalytic oxidation performance of the D600 and D700 catalysts also shows an improvement during the multiple NO oxidation test cycles. The NO oxidation activity of the D800, as shown in Fig. 1(d), is not enhanced by the multiple NO oxidation test cycles and the maximum NO oxidation ratio of D800 is far lower than the others. Table 1 listed the final NO oxidation performance data on all the catalysts after multiple NO oxidation test cycles. The $T_{10\%}$ of D500-cycle4, D600-cycle4, D700-cycle3 and D800-cycle2 are 247 °C, 268 °C, 268 °C and 282 °C, respectively. The T_P of D500-cycle4, D600-cycle4, D700-cycle3 and D800-cycle2 are 325 °C, 350 °C, 350 °C and 355 °C, respectively. The max of NO oxidation ratio of the D500-cycle4, D600-cycle4, D700-cycle3 and D800-cycle2 are 53.6%, 45.9%, 46.4% and 30.6%, respectively. Generally, the final NO catalytic oxidation performance of the D500-cycle4, D600-cycle4 and D700-cycle3 catalysts is improved during the long-time use (multiple NO oxidation test cycles) in the simulative diesel vehicle exhaust gases. Interestingly, the D700 sample maintains a strong catalytic NO oxidation performance either the initial D700-fresh or the final D700-cycle3. To study the reasons of catalytic performance differences of the catalysts, several characterizations and analysis were carried out. Due to the catalytic NO oxidation performance of the D800 is far lower than the

Table 1
The reaction light-off temperature ($T_{10\%}$), peak temperature (T_P) and maximum conversion ratio of NO to NO_2 for the fresh and long-time used catalysts.

Samples	$T_{10\%}$ (°C)	T_P (°C)	max of NO oxidation ratio (%)
D500-fresh	275	375	28.9
D500-cycle4	247	325	53.6
D600-fresh	280	380	35.5
D600-cycle4	268	350	45.9
D700-fresh	270	360	42.4
D700-cycle3	268	350	46.4
D800-fresh	284	365	32.0
D800-cycle2	282	355	30.6

others, the D800 sample is not further characterized and analyzed in the following sections.

3.2. Catalyst characterization

3.2.1. Platinum particle size

Platinum particle size plays an important role in NO catalytic oxidation performance [28,38]. Fig. 2 shows the transmission electron microscope (TEM), HAADF-STEM images and platinum particle size distribution of the three catalysts. The particle size distribution diagram is obtained by collecting and counting the Pt particle size from multiple HAADF-STEM images (as shown in Fig. S1 in Supporting Information). It can be seen from Fig. 2 that with increased treatment temperature, the average particle size of Pt particle increases rapidly from 1.40 nm of D500 to 14.04 nm of D600. When the treatment temperature reaches up to 700 °C, the average Pt particle size drops to approximately 1.82 nm, due to the high-temperature redispersion of Pt particles under high temperature and oxygen-rich conditions [39–42]. In previous studies [25,26] and our recent report [28], the catalyst with relatively larger Pt nanoparticles shows a better initial NO catalytic oxidation activity, due to larger Pt nanoparticles is helpful for maintaining the active species of

Pt^0 state during the preparation and using process. Furthermore, the relatively smaller platinum ($Pt^{\delta+}$) particles can be reduced to Pt^0 state more easily in the diesel vehicle exhaust gases and thus shows a superior final NO oxidation performance after long-time use (multiple NO oxidation reaction cycles) as reported by our previous works [28–30].

In combination with the catalytic NO oxidation activity results, it is interesting that although the Pt particle size of the D700 (~1.82 nm) is similar with the D500 (~1.40 nm), the initial NO oxidation performance of the D700-fresh is remarkably higher than that of the D500-fresh, and the final NO oxidation performance after long-time use of D700-cycle3 is slightly lower than that of the D500-cycle4. As shown in Fig. 2(a1) and 2 (a3), the deep black particles (marked by red ring) can be attributed to Pt nanoparticles, the light black particles with obvious lattice fringe are the Al_2O_3 nanocrystals. The shape of Pt nanoparticles of the D500 is irregular, and the majority of Pt nanoparticles do not show the lattice fringe, a few Pt nanoparticles show the lattice fringe. While for the D700 catalyst, lattice fringe is definitely observed in almost all the Pt nanoparticles. It indicates that the dominant structure of Pt nanoparticle (~1.40 nm) of the D-500 catalyst is amorphous; while for the high-temperature redispersion catalyst, D-700, the dominant structure of Pt nanoparticle (~1.82 nm) is nanocrystal. This is also confirmed by
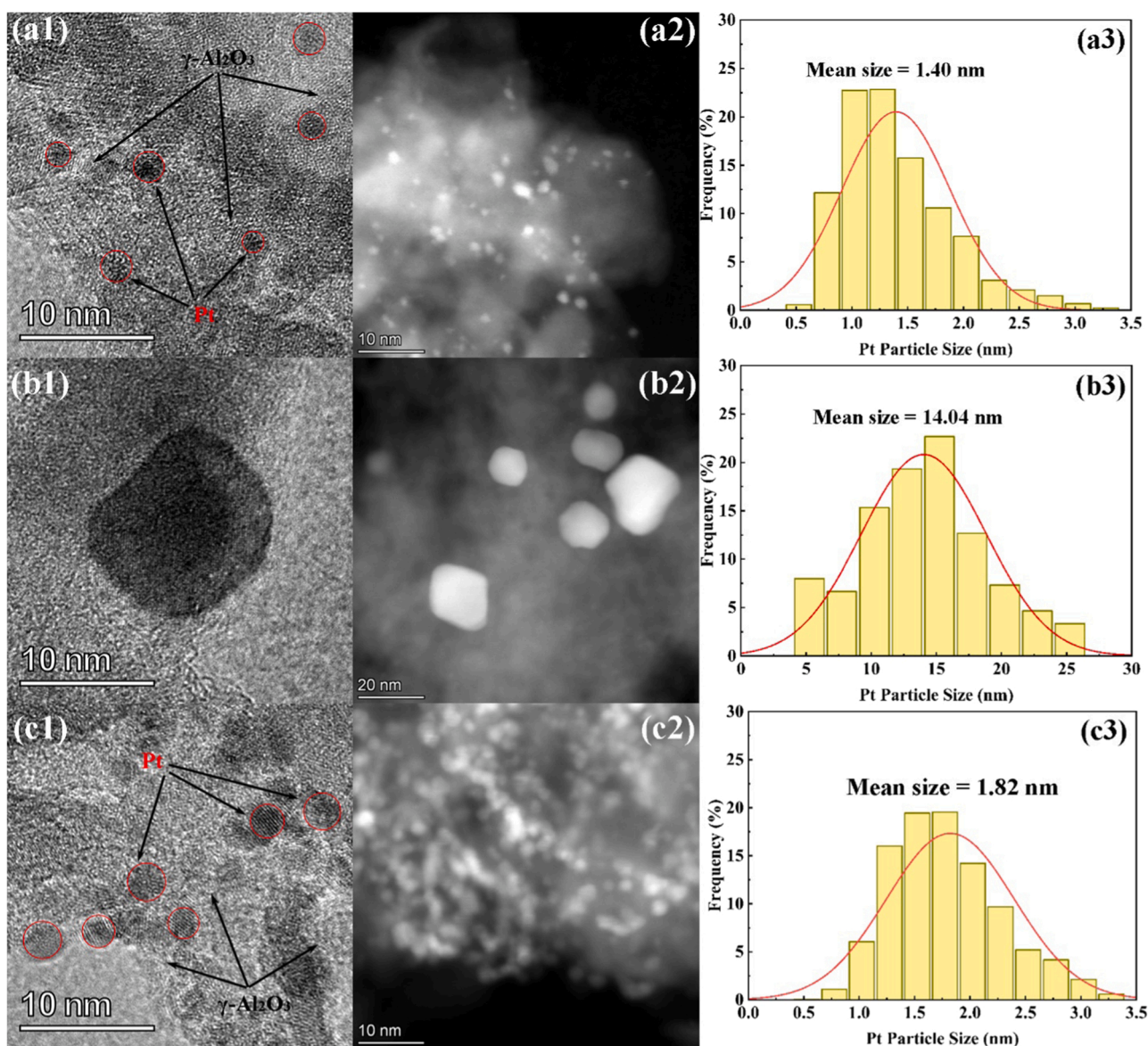
Fig. 2. TEM/HAADF-STEM images and Pt particle size of the D500 (a1, a2, a3), D600 (b1, b2, b3) and D700 (c1, c2, c3) catalysts.

further XRD experimental results in the next section. Thus, the differences of NO oxidation performance between the D500 and D700 maybe result from the difference between Pt amorphous nanoparticle (for D500) and nanocrystal (for D700), because of the mean Pt particle size of the D500 and D700 is almost the same (1.40 nm *vs.* 1.82 nm). Due to the fact that, compared with the crystal particle, the amorphous particle has more defects which can thus supply more active sites [43,44]. Therefore, the D500 catalyst with Pt amorphous nanoparticle should show a higher NO oxidation performance during the long-time use. In addition, it is worthy to note that the initial NO oxidation activity is mainly depending on the initial chemical states of Pt [25,26]. The catalyst with more Pt^0 active species, D-700, should display a higher initial NO oxidation activity, this is consistent with the catalytic performance results.

The nitrogen adsorption-desorption results (Fig. S2 and Table S1 in the Supporting Information) prove that the different calcination temperature does not affect the texture properties of the prepared catalysts. The BET surface area, pore volume and pore size of the D500, D600, D700 and D800 are similar. So texture properties are not the relevant factor impacting the catalytic activity and Pt particle size of the prepared catalysts.

3.2.2. XRD

Fig. 3 shows that all the samples display an obvious XRD characteristic diffraction peak at about 22.0°, it is because of the typical SiO_2 reflection (ICDD-PDF#29–0085). Meanwhile, the diffraction peaks at approximately 37.6°, 45.8°, 60.5°, and 66.8° are observed in all of the catalysts, which are attributed to the (311), (400), (511) and (440) crystal faces reflection of Al_2O_3 (ICDD-PDF#29–0063). The peak intensity at 45.8° and 66.8° of Al_2O_3 (400) and (440) crystal faces of all the samples are relatively strong, which is because of the overlap with Pt (200) and (220) XRD peaks. As it is well known that Pt (111), (200), (220) and (311) crystal face diffraction peaks are at approximately 39.8°, 46.2°, 67.5°, and 81.3°, respectively (ICDD-PDF#04–0802).

It is noteworthy to mention that the Pt (111) plane peak of the D500 catalyst is weak; however, for the D600 and D700 catalysts, the intensity of Pt (111) face is strong and the peak shape is sharp. The signals of undisturbed Pt (311) face of the D500 catalyst are not observed, while they are clearly visible for the other two catalysts, and the Pt (311) characteristic diffraction peaks of the D700 are stronger and sharper than that of the D600. It indicates that Pt particle on the D500 catalyst is mainly amorphous, for the D600 and D700 catalysts, Pt particle mainly exists in the form of nanocrystal. Pt crystallinity of the D500, D600 and D700 catalysts are 11.8%, 54.3% and 73.0%, respectively (as listed in Table 2). The crystal structure of high-temperature redispersion Pt
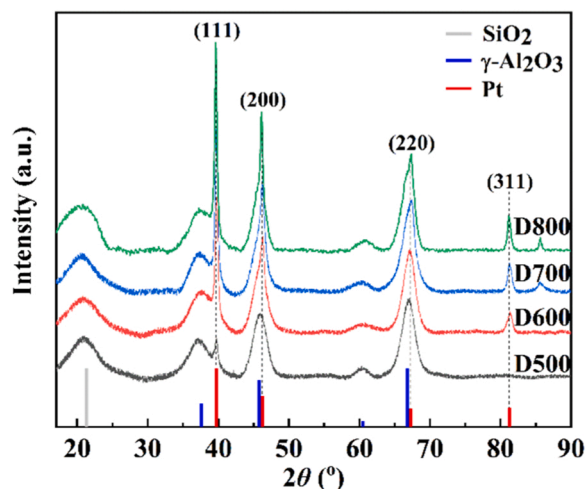
Fig. 3. XRD patterns of the D500, D600, D700 and D800 catalysts.

Table 2
The Pt average particle size, crystallinity and Pt species ratios on the D500, D600 and D700 catalysts.

Samples	Pt particle average size (nm)	Crystallinity (%)	Pt species ratios (wt%)		
			Pt^0	Pt^{2+}	Pt^{4+}
D500	1.40	11.8	13.21	36.89	49.90
D600	14.04	54.3	47.89	15.44	36.67
D700	1.82	73.0	63.71	17.39	18.90

nanocrystal of D700 catalyst is obviously more complete than that of the D500 and D600 catalyst, that is, the high-temperature redispersion of Pt would lead to more complete Pt crystal structures. This result is in line with the TEM results. Here we consider NO oxidation performance and Pt particle size of the prepared catalysts. Compared with the D600 catalyst, the D700 sample has remarkably smaller Pt particle size but shows similar NO oxidation performance, which may be because of the formation of Pt crystal which weakens NO catalytic oxidation activity. Because Pt crystal formation, in essence, is a process that Pt atoms arrange themselves in a regular fashion. Thus, the highly active corner, edge and defect sites of Pt nanoparticle are lost largely.[45,46] This is also the reason why the D700 has similar Pt mean size with the D500 (~1.82 nm *vs.* ~1.40 nm) but obviously lower final NO catalytic oxidation performance. Thus it implies that besides Pt particle size, the formation of Pt crystal is another factor for Pt/Al_2O_3 catalyst on NO catalytic oxidation.

3.2.3. XPS

The chemical state of Pt on catalyst is a key factor affecting the catalytic activity [47]. In order to study the chemical state of Pt on catalysts, X-ray photoelectron spectroscopy (XPS) was performed, and the results are shown in Fig. 4. It can be seen in Fig. 4(a) that a strong XPS peak at approximately 75.3 eV is observed in all catalysts, it is the Al^{3+} 2p core level spectrum and it is basically unchanged in all of the D500, D600, and D700 catalysts. While the electron binding energy signals of the catalysts at around 71.70, 73.10, and 78.50 eV are quite different (inset in Fig. 4(a)), which indicates that the Pt chemical state distributions of the three samples are quite different.

After deconvolution, besides the Al^{3+} 2p peak (at approximately 75.3 eV), all the catalysts show six Pt 4f peaks. The peak at around 75.15 and 78.50 eV are the 4$f_{7/2}$ and 4$f_{5/2}$ peak of Pt^{4+}, the 73.10 and 76.45 eV peaks are the 4$f_{7/2}$ and 4$f_{5/2}$ spin-spin splitting peak of Pt^{2+}, and the peak at around 71.70 and 75.05 eV are assigned to 4$f_{7/2}$ and 4$f_{5/2}$ peak of Pt^0. The XPS deconvolution data were listed detailedly in Table S2 in the Supporting Information and the percentages of Pt species in different chemical states were calculated and listed in Table 2. It can be seen that as the preparation temperature increases, the proportion of Pt^0 of the catalyst gradually increases, and meanwhile the proportion of $Pt^{\delta+}$ gradually decreases. Combining the results of TEM and XRD, it can be suggested that, for the D500 and D600, the content of Pt^0 increases with the increase of the Pt nanoparticle size. The reason is that relatively small Pt nanoparticles are easily oxidized to form $Pt^{\delta+}$ (PtO and PtO_2) during the preparation process, while relatively large particles are more difficult to be oxidized and hence has a higher Pt^0 content [48,49]. However, although the D700 catalyst has a smaller mean Pt particle size, Pt^0 content of the D700 catalyst is not reduced but increased. It indicates that the high-temperature treatment of Pt catalysts in air (oxygen-rich atmosphere) will lead to the transformation of $Pt^{\delta+}$ to Pt^0 species, not only in the sintering process (D600) but also in the redispersion process (D700). This phenomenon is also observed in the previous researches [50,51]. It may be attributed to the formation of highly complete Pt nanocrystal of the D700, which makes it difficult to be oxidized and hence has a higher Pt^0 content.

3.2.4. H₂-TPR

In order to study the oxidation-reduction performance of the
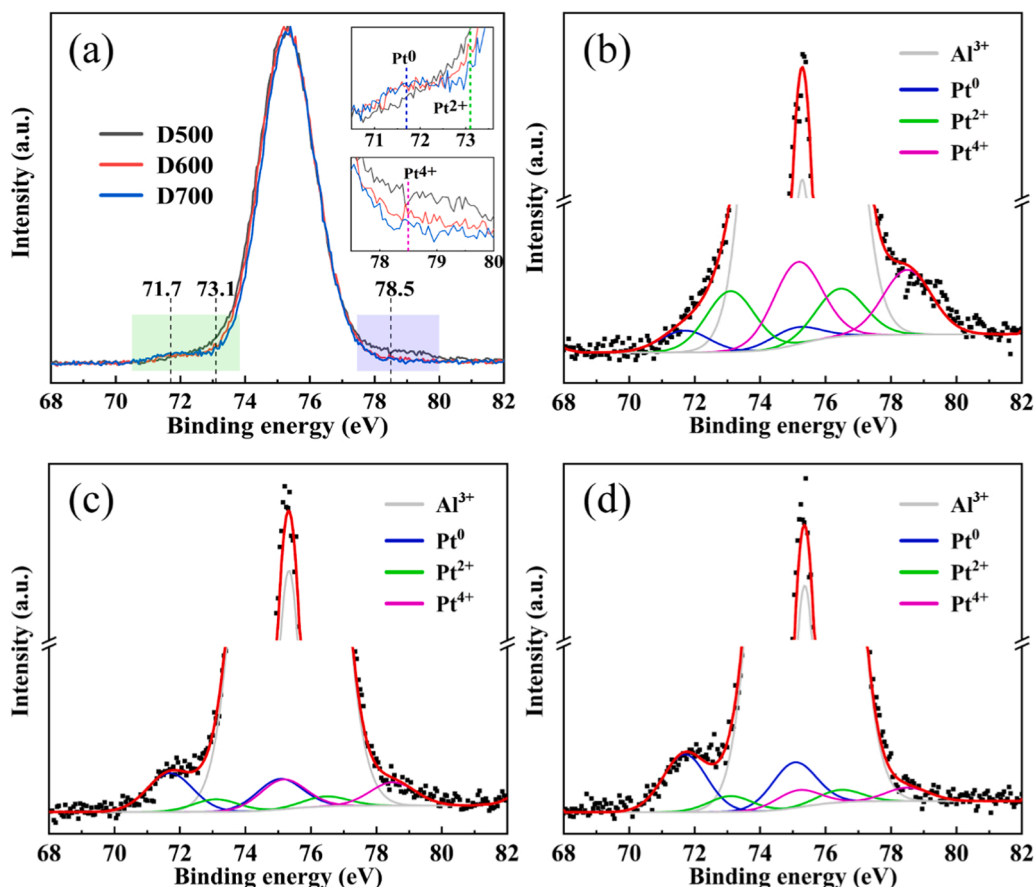
Fig. 4. XPS (Pt 4 *f*) spectra of the catalysts: (a) all the catalysts after normalization, (b) D500, (c) D600, (d) D700.

prepared Pt/Al$_2$O$_3$ catalysts, H$_2$ temperature-programmed reduction (H$_2$-TPR) was performed. As shown in Fig. 5, all of the three catalysts exhibit multiple H$_2$ consumption peaks at 25–650 °C. The H$_2$ consumption peak of α, before 250 °C, is attributed to the reduction of high-valence Pt$^{\delta+}$ species and the oxygen species strongly interacted with Pt on the catalyst [52]. For the D500 sample, the α peak is obviously larger than that of the D600 and D700 catalysts in sequence, it indicates that the reducible species (Pt$^{\delta+}$ species) of the D500 catalyst are more than the D600 and D700. The transformation of high-valence Pt$^{\delta+}$ to metallic Pt^0 species during the sintering (such as D600) and redispersion (such as D700) process is also observed in the previous researches [50,51], and this is in line with the results of XPS. Due to the large amount of high-valence Pt$^{\delta+}$ species and ultrafine particle size of platinum, the α peak of Pt$^{\delta+}$ reduction of the D500 is separate from the reduction of oxygen strongly interacted with Pt, so the α peak of D500 shows an obvious double-peak distribution ($\alpha1$ and $\alpha2$). The β peaks between 250 and 450 °C are attributed to the reduction of oxygen species which strongly interacts with the interface of Pt and the corresponding oxide support [34,53]. The γ peak at higher than 450 °C is attributed to the reduction of the Al$_2$O$_3$ support [54].
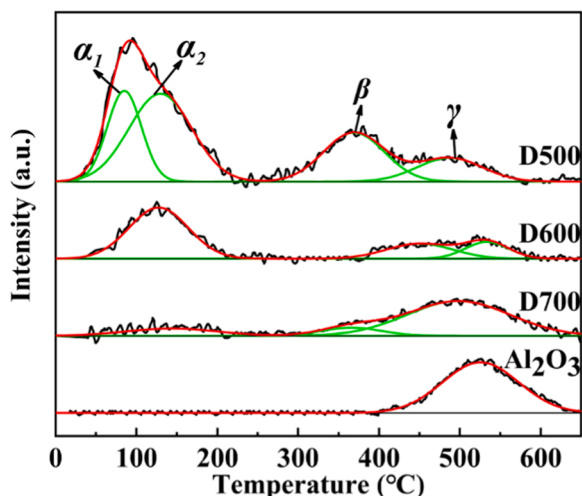
The H$_2$ consumption amount of each sample was calculated and listed in Table 3. It can be seen that the H$_2$ consumption amount of the catalysts obviously decreases with the treatment temperature in the low- and medium-temperature range, *i.e.*, 25–250 °C and 250–450 °C. Combining the results of XPS and TEM, it implies that with the increase of treatment temperature, Pt particle size gradually increases and crystallinity becomes more complete. It will result in the decrease of reducible species (Pt$^{\delta+}$ species) of the catalyst and hence the degradation of low- and medium-temperature redox properties; that is, the mobility of active species is decreased [55,56]. Therefore the larger Pt size and higher Pt crystallinity should make the Pt and Pt-Al$_2$O$_3$ interface of the catalyst more difficult to take part in the catalytic reaction.

3.2.5. NO-TPD

NO-TPD curves of the prepared catalysts are shown in Fig. 6. It can be seen that all the catalysts show three NO-TPD peaks. The α peak (80–200 °C) is attributed to the weak adsorbed NO, the β peak (200–450 °C) can ascribe to the unstable nitrate intermediates (such as nitrite and bridged nitrate), and the γ peak (450–800 °C) is characteristic of stable nitrate (chelated nitrate) [57–59]. It is obvious that the α and β peak of the D500 is markedly stronger than that of the D600 and

Fig. 5. H$_2$-TPR of the D500, D600 and D700 catalysts and Al$_2$O$_3$ support.

Table 3

H$_2$-TPR adsorption peak information of the catalysts and Al$_2$O$_3$ support.

Samples	D500				D600			D700			Al$_2$O$_3$
	α_1	α_2	β	γ	α	β	γ	α	β	γ	γ
Temperature (℃)	85	130	369	488	128	450	534	143	366	498	526
Area	62	111	60	31	61	20	14	13	10	72	77
H$_2$ consumption (μmol)	0.44	0.78	0.42	0.22	0.43	0.14	0.10	0.09	0.07	0.51	0.54
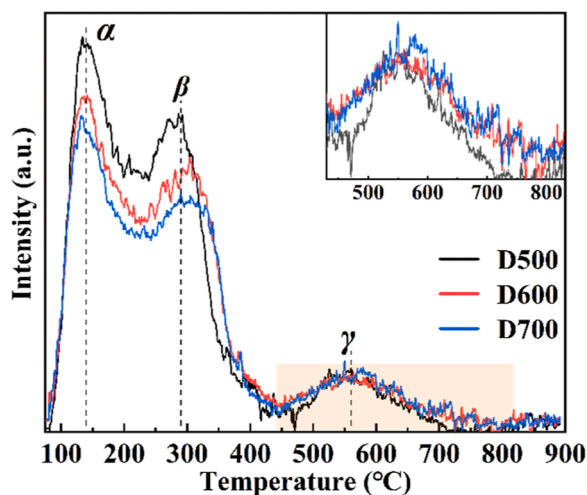
Fig. 6. NO-TPD curves of the D500, D600 and D700 catalysts.

D700 catalysts in sequence. Meanwhile, the γ peak of the D500 is slightly weaker than that of the D600 and D700 catalysts in sequence. Thus, it can be suggested that the smaller size and lower crystallinity of platinum particle of the catalysts are beneficial for the formation of unstable nitrate intermediates and hence promoting NO catalytic oxidation. The larger size and higher crystallinity of platinum particle should be beneficial for the generation stable nitrates and therefore disadvantaging NO catalytic oxidation.

3.3. NO oxidation reaction pathway

To further study the reaction pathway of NO catalytic oxidation on the catalysts, *in-situ* FTIR spectra was used. Fig. 7 shows the *in-situ* FTIR spectra of the chemical reaction of NO and O$_2$ on catalyst (NO-only conditions) under different reaction temperatures. It is well known that the FTIR peaks at approximately 1243 cm^{-1} and 1636 cm^{-1} can be attributed to the characteristic absorption of bidentate nitrite and bridged nitrate, respectively [60–62]; and the multiple absorption peaks appeared at 1450–1560 cm^{-1} are mainly because of the formation of monodentate nitrate and bidentate nitrate species on catalyst surface [63–65]. For all the catalysts, as shown in Fig. 7, the peak intensities of all the nitrite and/or nitrate intermediates increase with the reaction temperature, which implies that the NO catalytic oxidation rete is
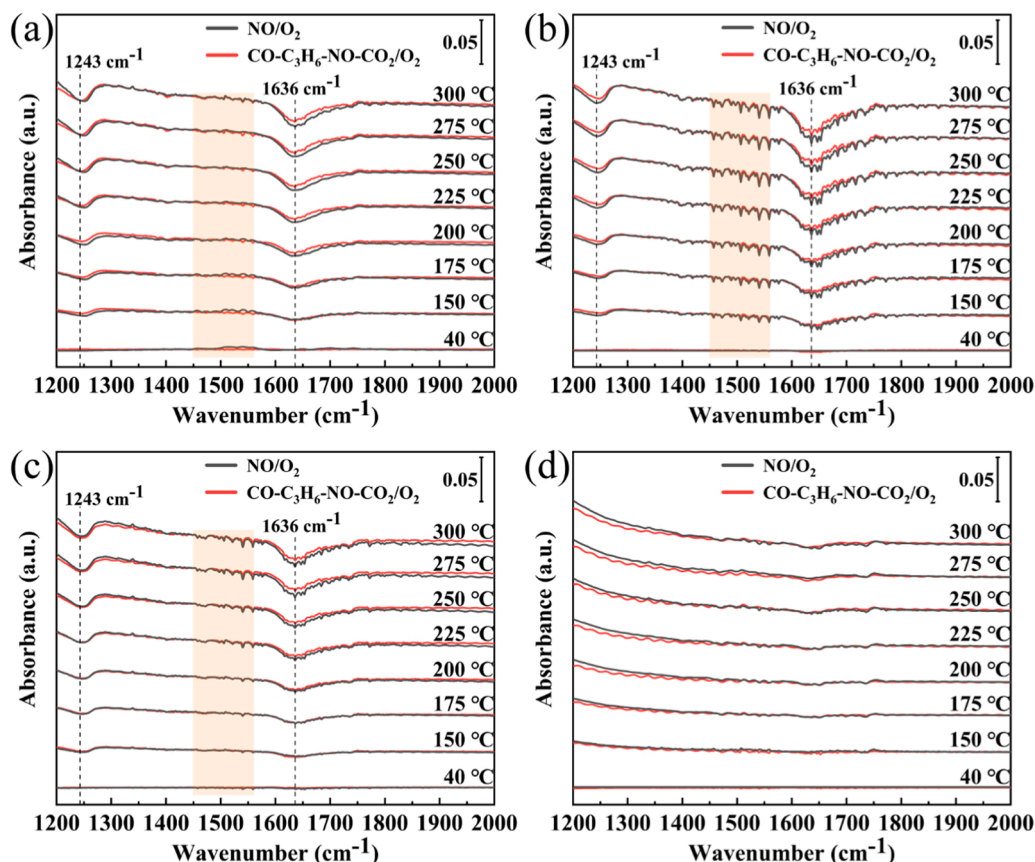
Fig. 7. *In-situ* FTIR spectra of the (a) D500, (b) D600, (c) D700 catalysts and (d) KBr under NO/O$_2$ and CO-C$_3$H$_6$-NO-CO$_2$/O$_2$ conditions.

directly related to the reaction temperature, and this is in line with the catalytic activity results in Section 3.1.

For the D500 catalyst (Fig. 7(a)), both the bidentate nitrite (1243 cm^{-1}) and bridged nitrate (1636 cm^{-1}) are detected, which are the typical reaction intermediates of NO oxidation, no other nitrite/nitrate species were observed. Interestingly, besides bidentate nitrite and bridged nitrate species, chelated nitrate species (1450–1560 cm^{-1}) are affirmatively generated on the D600 catalyst in Fig. 7(b), and the formation amounts of chelated nitrates obviously increase with NO oxidation rate and reaction temperature. Moreover, for the D700 catalyst in Fig. 7(c), chelated nitrate species (1450–1560 cm^{-1}) are not observed at low-temperature range (lower than 225 °C), and the intensity of FTIR peak of the chelated nitrate at over 225 °C is markedly weaker than that of the D600 catalyst. By contrasting Pt particle size of the D500 with D600 catalyst (1.40 nm *vs.* 14.04 nm), it is clear that the larger size of Pt particle of catalyst will lead to the generation of chelated nitrate species. Comparing the D500 and D700, it can be suggested that when the particle size of Pt is similar (1.40 nm *vs.* 1.82 nm), the higher crystallinity of Pt particle will cause the formation of chelated nitrates more easily. It is proved that the thermal stability of nitrite/nitrate species on Al$_2$O$_3$-supported catalyst surface follow the sequence of nitrite < bridged nitrate < bidentate nitrate ≈ monodentate nitrate.[66] It means that compared with bidentate nitrite and bridged nitrate, chelated nitrates (monodentate nitrate and bidentate nitrate) shows higher thermal stability, which is more difficult to be decomposed and desorbed from catalyst surface to generate NO$_2$.

Furthermore, as shown in Fig. 7, the *in-situ* FTIR data of all the catalysts under simulated diesel exhaust environments (containing 1000 ppm CO, 330 ppm C$_3$H$_6$, 1000 ppm NO, 3000 ppm CO$_2$) were also collected. It shows the same trend with that of the NO-only conditions, which indicates that the presence of CO and C$_3$H$_6$ in diesel exhaust does not influence the reaction pathway of NO oxidation and the NO catalytic oxidation activity on the prepared Pt-based catalysts. This is because of the relatively high $T_{10\%}$ of NO oxidation (higher than 247 °C, as shown in Fig. 1) on the prepared catalysts. While the $T_{10\%}$ of catalytic CO and C$_3$H$_6$ oxidation on Pt-based catalysts are generally lower than 200 °C, as reported by our previous work [29,34–36]. Interestingly, the FTIR peak intensity of bidentate nitrite (1243 cm^{-1}) and bridged nitrate (1636 cm^{-1}) on all the prepared catalysts under NO-only conditions are slightly stronger than that under the simulated diesel exhaust conditions. It implies that the competitive adsorption of CO/C$_3$H$_6$ will slightly restrain the adsorption and transformation of NO on the catalysts. Besides, the reaction intermediates of CO/C$_3$H$_6$ oxidation are not observed. This is mainly because of the quick CO/C$_3$H$_6$ oxidation (the direct reaction of CO/C$_3$H$_6$ and oxygen on noble metal sites), there is no adsorbed CO and C$_3$H$_6$ accumulation on the noble metal sites.[67,68].

Additionally, because the catalyst is in the atmosphere when the DOC is in idle status. To further study the effects of pre-adsorbed oxygen on catalyst and NO catalytic oxidation pathway, the *in-situ* FTIR tests of all the catalysts were performed under the conditions of adding O$_2$ first and then adding NO (as shown in Fig. S3 in Supporting Information). Generally, the trends of NO catalytic reaction on the prepared catalysts are similar with the results of adding NO first and then adding O$_2$ (Fig. 7). Noteworthily, the pre-adsorption of oxygen leads to the decrease of nitrite/bridged nitrate and the increase of chelated nitrate. This is because oxygen pre-adsorbed on the catalyst Pt sites will restrain the adsorption of NO; on the other hand, the presence of adsorbed oxygen will inhibit the conversion of stable nitrate species (chelated nitrate) to less stable nitrite/bridged nitrate species [66].

Thus, based on the above results, one can see that nitrite and bridging nitrate are the mainly intermediates for NO catalytic oxidation on Pt/Al$_2$O$_3$ catalyst. If the decomposition and desorption of nitrite and bridging nitrate intermediates from catalyst surface cannot effectively occur, then that will be converted to chelated nitrates. The chelated nitrates are more stable and harder to decompose to generate NO$_2$, and hence restrain the NO catalytic oxidation reaction. Thus, it shows that

smaller platinum particle is conducive to decomposition of nitrite/nitrate intermediates and hence facilitate NO oxidation reactions. The higher crystallinity of platinum particle leads to generation and accumulation of chelated nitrates consequently cover the catalyst active sites. It is in line with the NO-TPD results. The competitive adsorption of CO/C$_3$H$_6$ in diesel exhaust will slightly restrain the adsorption and transformation of NO on the catalysts, but not obviously influence the NO oxidation pathway and NO catalytic oxidation activity.

4. Conclusion

Our results show that high-temperature redispersion of platinum nanoparticle on Pt/Al$_2$O$_3$ catalyst play an important role in both diesel exhaust NO catalytic oxidation activity and reaction pathways. The high-temperature redispersion not only can decrease the mean size of platinum particle, but also increase the crystallinity of platinum particle (as shown in TEM and XRD results). The smaller platinum nanoparticles are disadvantageous to maintain Pt^0 active phase in the preparation process but conducive to the reduction of high-valence Pt$^{\delta+}$ to Pt^0 during the reaction. The higher crystallinity of platinum particle on catalyst is beneficial for maintaining Pt^0 state but adverse to the reduction of Pt$^{\delta+}$ species during the reaction. NO oxidation on Pt/Al$_2$O$_3$ catalyst is primarily through the pathways of nitrite and bridging nitrate intermediates. When the decomposition of intermediates are not able to occur promptly, that will be converted to more stable chelated nitrates, which are harder to decompose and hence restrain the catalytic NO oxidation reaction. Moreover, the high-temperature redispersion of Pt/Al$_2$O$_3$ catalyst results in a smaller Pt particle size and higher Pt crystallinity. The former is conducive to the decomposition of nitrite/nitrate intermediates and therefore facilitate the NO catalytic oxidation reaction. Meanwhile, the latter will lead to the generation and accumulation of chelated nitrates consequently cover the active sites and restrain NO oxidation reaction.

References

[1] X. Auvray, M. Arvanitidou, Å. Högström, J. Jansson, S. Fouladvand, L. Olsson, Comparative study of SO_2 and SO_2/SO_3 poisoning and regeneration of Cu/BEA and Cu/SSZ-13 for NH_3-SCR, Emiss. Control Sci. Technol. 7 (2021) 232–246.

[2] Q. Zhang, J. Zhang, Z. Song, P. Ning, H. Li, X. Liu, A novel and environmentally friendly SO_4^{2-}/CeO_2 catalyst for the selective catalytic reduction of NO with NH_3, J. Ind. Eng. Chem. 34 (2016) 165–171.

[3] Z. Yang, W. Hu, N. Zhang, Y. Li, Y. Liao, Facile synthesis of ceria-zirconia solid solutions with cubic-tetragonal interfaces and their enhanced catalytic performance in diesel soot oxidation, J. Catal. 377 (2019) 98–109.

[4] M. Václavík, V. Novák, J. Březina, P. Kočí, G. Gregori, D. Thompsett, Effect of diffusion limitation on the performance of multi-layer oxidation and lean NOx trap catalysts, Catal. Today 273 (2016) 112–120.

[5] Z. Yang, L. Luo, L. Tang, Z. Zhou, Z. Zhou, Y. Li, Trimesic acid assisted synthesis of cerium-manganese oxide for catalytic diesel soot elimination: Enhancement of thermal aging resistibility, Fuel 278 (2020), 118369.

[6] Y. Xie, E. Rodrigues, N. Furtado, A. Matynia, T. Arlt, P. Rodatz, P. Da Costa, Aging of commercial diesel oxidation catalysts: a preliminary structure/reactivity study, Top. Catal. 59 (2016) 1039–1043.

[7] Z. Yang, N. Zhang, H. Xu, Y. Li, L. Ren, Y. Liao, Y. Chen, Boosting diesel soot catalytic combustion via enhancement of solid(catalyst)-solid(soot) contact by tailoring micrometer scaled sheet-type agglomerations of CeO_2-ZrO_2 catalyst, Combust. Flame 235 (2022), 111700.

[8] R.K. More, N.R. Lavande, P.M. More, Copper supported on Co substituted hydroxyapatite for complete oxidation of diesel engine exhaust and VOC, Mol. Catal. 474 (2019), 110414.

[9] H. Xu, J. Liu, Z. Zhang, S. Liu, Q. Lin, Y. Wang, S. Dai, Y. Chen, Design and synthesis of highly-dispersed WO_3 catalyst with highly effective NH_3–SCR activity for NOx abatement, Acs Catal. 9 (2019) 11557–11562.

[10] A. Arvajová, P. Kočí, Impact of PtOx formation in diesel oxidation catalyst on NO_2 yield during driving cycles, Chem. Eng. Sci. 158 (2017) 181–187.

[11] A. Grossale, I. Nova, E. Tronconi, Ammonia blocking of the "Fast SCR" reactivity over a commercial Fe-zeolite catalyst for Diesel exhaust aftertreatment, J. Catal. 265 (2009) 141–147.

[12] A. Winkler, D. Ferri, M. Aguirre, The influence of chemical and thermal aging on the catalytic activity of a monolithic diesel oxidation catalyst, Appl. Catal. B: Environ. 93 (2009) 177–184.

[13] P.H. Ho, J. Shao, D. Yao, R.F. Ilmasani, M.A. Salam, D. Creaser, L. Olsson, The effect of Pt/Pd ratio on the oxidation activity and resistance to sulfur poisoning for Pt-Pd/BEA diesel oxidation catalysts with high siliceous content, J. Environ. Chem. Eng. 10 (2022), 108217.

[14] D. Fang, K. Qi, F. Li, F. He, J. Xie, Excellent sulfur tolerance performance over Fe-SO_4/TiO_2 catalysts for NH_3-SCR: Influence of sulfation and Fe-based sulfates, J. Environ. Chem. Eng. 10 (2022), 107038.

[15] C. Yang, K. Zhang, Y. Zhang, Gj Peng, M. Yang, J. Wen, Y. Xie, F. Xia, L. Jia, Q. Zhang, An environmental and highly active Ce/Fe-Zr-SO_4^{2-} catalyst for selective catalytic reduction of NO with NH_3: The improving effects of CeO_2 and SO_4^{2-}, J. Environ. Chem. Eng. 9 (2021), 106799.

[16] Y. Liang, X. Ding, Z. Du, J. Wang, M. Zhao, Y. Dan, L. Jiang, Y. Chen, Low-temperature performance controlled by hydroxyl value in polyethylene glycol enveloping Pt-based catalyst for CO/C_3H_6/NO oxidation, Mol. Catal. 484 (2020), 110740.

[17] X. Auvray, A. Thuault, Effect of microwave drying, calcination And Aging of Pt/Al_2O_3 on platinum dispersion, Catalysts 8 (2018) 348.

[18] A.P. Wong, E.A. Kyriakidou, T.J. Toops, J.R. Regalbuto, The catalytic behavior of precisely synthesized Pt–Pd bimetallic catalysts for use as diesel oxidation catalysts, Catal. Today 267 (2016) 145–156.

[19] D.-E. Lee, D. Jin Kim, V. Devthade, W.-K. Jo, S. Tonda, Size-dependent selectivity and activity of highly dispersed sub-nanometer Pt clusters integrated with P25 for CO_2 photoreduction into methane fuel, Appl. Surf. Sci. 584 (2022), 152532.

[20] Z. Yuan, Z. Chen, J. Mao, R. Zhou, The size effect and high activity of nanosized platinum supported catalysts for low temperature oxidation of volatile organic compounds, Chin. J. Chem. Eng. 39 (2021) 135–143.

[21] S. Luo, X. Wu, B. Jin, S. Liu, R. Ran, Z. Si, D. Weng, Size effect of Pt nanoparticles in acid-assisted soot oxidation in the presence of NO, J. Environ. Sci. 94 (2020) 64–71.

[22] S. Neumann, T. Gutmann, G. Buntkowsky, S. Paul, G. Thiele, H. Sievers, M. Bäumer, S. Kunz, Insights into the reaction mechanism and particle size effects of CO oxidation over supported Pt nanoparticle catalysts, J. Catal. 377 (2019) 662–672.

[23] K. Yu, J. Deng, Y. Shen, A. Wang, L. Shi, D. Zhang, Efficient catalytic combustion of toluene at low temperature by tailoring surficial Pt^0 and interfacial Pt-Al(OH)x species, iScience 24 (2021), 102689.

[24] X. Li, Y.-R. Liu, W.-M. Liao, A.-P. Jia, Y.-J. Wang, J.-Q. Lu, M.-F. Luo, Synergistic roles of Pt^0 and Pt^{2+} species in propane combustion over high-performance Pt/AlF_3 catalysts, Appl. Surf. Sci. 475 (2019) 524–531.

[25] A.D. Smeltz, W.N. Delgass, F.H. Ribeiro, Oxidation of NO with O_2 on Pt(111) and pt (321) large single crystals, Langmuir 26 (2010) 16578–16588.

[26] L. Olsson, E. Fridell, The influence of Pt oxide formation and Pt dispersion on the reactions $NO_2 \Leftrightarrow NO+1/2\ O_2$ over Pt/Al_2O_3 and Pt/BaO/Al_2O_3, J. Catal. 210 (2002) 340–353.

[27] L.M. Carballo, E.E. Wolf, Crystallite size effects during the catalytic oxidation of propylene on Pt/γ-Al_2O_3, J. Catal. 53 (1978) 366–373.

[28] Z. Chen, D. Luo, H. Zhang, N. Zhang, J. Li, B. Gao, R. Qiu, Y. Li, Z. Yang, Reaction pathway of nitric oxide oxidation on nano-sized Pt/SiO_2 catalysts for diesel exhaust purification, Mol. Catal. 516 (2021), 111991.

[29] Z. Yang, J. Li, H. Zhang, Y. Yang, M. Gong, Y. Chen, Size-dependent CO and propylene oxidation activities of platinum nanoparticles on the monolithic Pt/TiO_2-YOx diesel oxidation catalyst under simulative diesel exhaust conditions, Catal. Sci. Technol. 5 (2015) 2358–2365.

[30] Z. Yang, N. Zhang, Y. Cao, M. Gong, M. Zhao, Y. Chen, Effect of yttria in Pt/TiO_2 on sulfur resistance diesel oxidation catalysts: enhancement of low-temperature activity and stability, Catal. Sci. Technol. 4 (2014) 3032–3043.

[31] X. Auvray, L. Olsson, Stability and activity of Pd-, Pt- and Pd–Pt catalysts supported on alumina for NO oxidation, Appl. Catal. B: Environ. 168–169 (2015) 342–352.

[32] X. Auvray, T. Pingel, E. Olsson, L. Olsson, The effect gas composition during thermal aging on the dispersion and NO oxidation activity over Pt/Al_2O_3 catalysts, Appl. Catal. B: Environ. 129 (2013) 517–527.

[33] E. Ruckenstein, M.L. Malhotra, Splitting of platinum crystallites supported on thin, nonporous alumina films, J. Catal. 41 (1976) 303–311.

[34] Z.-Z. Yang, Y. Yang, M. Zhao, M.-C. Gong, Y.-Q. Chen, Enhanced sulfur resistance of Pt-Pd/CeO_2-ZrO_2-Al_2O_3 commercial diesel oxidation catalyst by SiO_2 surface cladding, Acta Phys. -Chim. Sin. 30 (2014) 1187–1193.

[35] Z. Yang, Y. Li, Y. Liao, Y. Li, N. Zhang, Preparation and properties of the Pt/SiO_2-Al_2O_3 sulfur resistance diesel oxidation catalyst (IN CHINESE), Huanjing Huaxue (Environ. Chem.) 35 (2016) 1682–1689.

[36] Z. Yang, N. Zhang, Y. Cao, Y. Li, Y. Liao, Y. Li, M. Gong, Y. Chen, Promotional effect of lanthana on the high-temperature thermal stability of Pt/TiO_2 sulfur-resistant diesel oxidation catalysts, Rsc Adv. 7 (2017) 19318–19329.

[37] B.A. Rozenberg, R. Tenne, Polymer-assisted fabrication of nanoparticles and nanocomposites, Prog. Polym. Sci. 33 (2008) 40–112.

[38] F.J. Gracia, L. Bollmann, E.E. Wolf, J.T. Miller, A.J. Kropf, In situ FTIR, EXAFS, and activity studies of the effect of crystallite size on silica-supported Pt oxidation catalysts, J. Catal. 220 (2003) 382–391.

[39] X. Zhou, Y. Zhang, J. Wang, DFT study on the regeneration of Pt/γ-Al_2O_3 catalyst: the effect of chlorine on the redispersion of metal species, Appl. Surf. Sci. 545 (2021), 148988.

[40] J. Jones, H. Xiong, T. DeLaRiva Andrew, J. Peterson Eric, H. Pham, R. Challa Sivakumar, G. Qi, S. Oh, H. Wiebenga Michelle, I. Pereira Hernández Xavier, Y. Wang, K. Datye Abhaya, Thermally stable single-atom platinum-on-ceria catalysts via atom trapping, Science 353 (2016) 150–154.

[41] T. Wu, X. Pan, Y. Zhang, Z. Miao, B. Zhang, J. Li, X. Yang, Investigation of the redispersion of Pt nanoparticles on polyhedral ceria nanoparticles, J. Phys. Chem. Lett. 5 (2014) 2479–2483.

[42] M. Hatanaka, N. Takahashi, N. Takahashi, T. Tanabe, Y. Nagai, A. Suda, H. Shinjoh, Reversible changes in the Pt oxidation state and nanostructure on a ceria-based supported Pt, J. Catal. 266 (2009) 182–190.

[43] K. Kim, T. Kang, M. Kim, J. Kim, Exploring the intrinsic active sites and multi oxygen evolution reaction step via unique hollow structures of nitrogen and sulfur co-doped amorphous cobalt and nickel oxides, Chem. Eng. J. 426 (2021), 130820.

[44] Y. Ma, R. Wang, H. Wang, V. Linkov, S. Ji, Evolution of nanoscale amorphous, crystalline and phase-segregated PtNiP nanoparticles and their electrocatalytic effect on methanol oxidation reaction, Phys. Chem. Chem. Phys. 16 (2014) 3593–3602.

[45] Y. Tuo, Y. Meng, C. Chen, D. Lin, X. Feng, Y. Pan, P. Li, D. Chen, Z. Liu, Y. Zhou, J. Zhang, Partial positively charged Pt in Pt/$MgAl_2O_4$ for enhanced dehydrogenation activity, Appl. Catal. B: Environ. 288 (2021), 119996.

[46] C. Hao, J. Gan, Y. Cao, W. Luo, W. Chen, G. Qian, X. Zhou, X. Duan, Crucial size effects of atomic-layer-deposited Pt catalysts on methanol electrooxidation, Catal. Today 364 (2021) 157–163.

[47] L. Olsson, H. Persson, E. Fridell, M. Skoglundh, B. Andersson, A kinetic study of NO oxidation and NOx storage on Pt/Al_2O_3 and Pt/BaO/Al_2O_3, J. Phys. Chem. B 105 (2001) 6895–6906.

[48] R. Burch, P.K. Loader, Investigation of methane oxidation onPt/Al_2O_3 catalysts under transient reaction conditions, Appl. Catal. A: Gen. 122 (1995) 169–190.

[49] R.F. Hicks, H. Qi, M.L. Young, R.G. Lee, Effect of catalyst structure on methane oxidation over palladium on alumina, J. Catal. 122 (1990) 295–306.

[50] T. Tanabe, Y. Nagai, K. Dohmae, H. Sobukawa, H. Shinjoh, Sintering and redispersion behavior of Pt on Pt/MgO, J. Catal. 257 (2008) 117–124.

[51] J. Li, Y. Zhang, T. Yi, Z. Zhang, Z. Miao, L. Sun, Z. Zhang, X. Yang, The redispersion behaviour of Pt on the surface of Fe_2O_3, Rsc Adv. 6 (2016) 25894–25899.

[52] C. Lin, Z. Yang, H. Pan, J. Cui, Z. Lv, X. liu, P. Tian, Z. Xiao, P. Li, J. Xu, Y.-F. Han, Ce-introduced effects on modification of acidity and Pt electronic states on Pt-Sn/γ-Al_2O_3 catalysts for catalytic reforming, Appl. Catal. A: Gen. 617 (2021) 118116.

[53] Y. Liang, C. Ou, H. Zhang, X. Ding, M. Zhao, J. Wang, Y. Chen, Advanced insight into the size effect of PtPd nanoparticles on NO oxidation by in situ FTIR spectra, Ind. Eng. Chem. Res. 57 (2018) 3887–3897.

[54] M.J. Tiernan, O.E. Finlayson, Effects of ceria on the combustion activity and surface properties of Pt/Al_2O_3 catalysts, Appl. Catal. B: Environ. 19 (1998) 23–35.

[55] J. Waikar, P. More, Complete oxidation of CO and propene as model component of diesel exhaust and VOC using manganese oxide supported on octahedral (AlO_6^{3-})-Ce^{3+}, Appl. Surf. Sci. Adv. 7 (2022), 100204.

[56] N.R. Lavande, R.K. More, P.M. More, Mg modified MnO_x-$CeO_{2-\delta}$ catalyst for low temperature complete oxidation of simulated diesel engine exhaust, Appl. Surf. Sci. 502 (2020), 144299.

[57] P. Anguita, J.M. García-Vargas, F. Gaillard, E. Iojoiu, S. Gil, A. Giroir-Fendler, Effect of Na, K, Ca and P-impurities on diesel oxidation catalysts (DOCs), Chem. Eng. J. 352 (2018) 333–342.

[58] S. Koukiou, M. Konsolakis, R.M. Lambert, I.V. Yentekakis, Spectroscopic evidence for the mode of action of alkali promoters in Pt-catalyzed de-NOx chemistry, Appl. Catal. B: Environ. 76 (2007) 101–106.

[59] C. Sedlmair, K. Seshan, A. Jentys, J.A. Lercher, Elementary steps of NOx adsorption and surface reaction on a commercial storage-reduction catalyst, J. Catal. 214 (2003) 308–316.

[60] Q. Zhang, Y. Zhang, T. Zhang, H. Wang, Y. Ma, J. Wang, P. Ning, Influence of preparation methods on iron-tungsten composite catalyst for NH_3-SCR of NO: the active sites and reaction mechanism, Appl. Surf. Sci. 503 (2020), 144190.

[61] F. Zhang, S. Zhang, N. Guan, E. Schreier, M. Richter, R. Eckelt, R. Fricke, NO SCR with propane and propene on Co-based alumina catalysts prepared by co-precipitation, Appl. Catal. B: Environ. 73 (2007) 209–219.

[62] K. Hadjiivanov, H. Knözinger, Species formed after NO adsorption and NO + O_2 co-adsorption on TiO_2: an FTIR spectroscopic study, Phys. Chem. Chem. Phys. 2 (2000) 2803–2806.

[63] A. Kvasničková, P. Kočí, Y. Ji, M. Crocker, Effective model of NOx adsorption and desorption on PtPd/CeO_2-ZrO_2 passive NOx adsorber, Catal. Lett. 150 (2020) 3223–3233.

[64] M. Kantcheva, M. Milanova, S. Mametsheripov, In situ FT-IR spectroscopic investigation of gold supported on tungstated zirconia as catalyst for CO-SCR of NOx, Catal. Today 191 (2012) 12–19.

[65] M. Kantcheva, I. Cayirtepe, Routes of formation and composition of NOx complexes adsorbed on palladium-promoted tungstated zirconia, J. Mol. Catal. A: Chem. 247 (2006) 88–98.

[66] S.J. Huang, A.B. Walters, M.A. Vannice, TPD, TPR and DRIFTS studies of adsorption and reduction of NO on La_2O_3 dispersed on Al_2O_3, Appl. Catal. B: Environ. 26 (2000) 101–118.

[67] X. Feng, Z. Wang, L. Mu, Z. Chen, J. Liang, C. Xiao, The different evolution behaviors of carbonate-like species on Pt/CeO2 and Pt/Al2O3 by in situ DRIFTS-MS study, Catal Today, https://doi.org/10.1016/j.cattod.2021.11.009 (2021).

[68] Z. Tan, M. Haneda, H. Kitagawa, B. Huang, Slow synthesis methodology-directed immiscible octahedral Pd_xRh_{1-x} dual-atom-site catalysts for superior three-way catalytic activities over Rh, Angew. Chem. Int. Ed. 61 (2022), e202202588.